In-situ impact analysis during fatigue tests of open-hole carbon fibre reinforced polymer specimens

Zarouchas, Dimitrios; van Dien, Casper; Eleftheroglou, Nick

DOI
10.1016/j.jcomc.2021.100199

Publication date
2021

Document Version
Final published version

Published in
Composites Part C: Open Access

Citation (APA)
Zarouchas, D., van Dien, C., & Eleftheroglou, N. (2021). In-situ impact analysis during fatigue tests of open-hole carbon fibre reinforced polymer specimens. *Composites Part C: Open Access*, *6*, Article 100199. https://doi.org/10.1016/j.jcomc.2021.100199

Composites Part C: Open Access 6 (2021) 100199

Contents lists available at ScienceDirect

Composites Part C: Open Access

journal homepage: www.sciencedirect.com/journal/composites-part-c-open-access

In-situ impact analysis during fatigue tests of open-hole carbon fibre reinforced polymer specimens

Dimitrios Zarouchas *, Casper van Dien, Nick Eleftheroglou

Structural Integrity & Composites Group, Aerospace Engineering Faculty, Delft University of Technology, Delft, 2629 HS, The Netherlands

ARTICLE INFO

Keywords:
In-situ impact
Fatigue
Damage diagnostics

ABSTRACT

This paper presents the results for an experimental campaign of in-situ impact during tension-tension fatigue loading for open-hole carbon fibre reinforced polymer specimens. High-speed low energy impact was introduced to the specimen with the use of a canon, which was attached to testing bench enabling the impact without the need to remove the specimens from the test bench. Digital Image Correlation, C-scan and Acoustic Emission were utilized to record health monitoring data for damage diagnostics. A strain-based criterion was used to identify a common threshold for the timing of impact ensuring a fair comparison between the different tests. The results indicate that while an impact causes the total amount of damage to increase as one would expect, it does not necessarily increase the damage level in the critical area where final fracture occurs. A dependence on the moment of impact with the fatigue failure was found for specimens subjected to impact before the initiation of the fatigue loading. In contrast, impacting specimens in the presence of fatigue damage had no detrimental effect on the fatigue life, although it was observed that the damaged area was enlarged. Overall, the paper showcases the need to study systemically the effect of in-situ impact on the fatigue life in order to understand better the implications that may be introduced to the integrity of a composite structure.

1. Introduction

Composite structures are increasingly used in commercial aviation replacing the traditional aerospace aluminium alloys, with some of the newest generations of passenger aircraft having over half of their structural weight made from composites. Due to their distinct nature, a different design and damage tolerance philosophy has to be taken into account as their anisotropic behaviour and variety of failure mechanisms foster complex damage patterns and stochastic damage degradation processes [1,2].

Fatigue of composite structures has been in the centre of the research activities the last six decades, where the research community has tried to model the phenomenon of damage accumulation and develop predictive tools [3]. Extensive experimental campaigns for different material types and lay-up configurations and a considerable number of models emerged from those activities and revealed that the fatigue damage process is a multi-state degradation procedure where several damage mechanisms occur, interact and act synergistically. The idea of the multi-state process goes back to the '80 s, where Reifsneider et al. described the damage accumulation as a three-stage process [4]. It was the first time proposed in literature that the prediction of strength and life of a composite structure should be based on the damage accumulation process. Ever since, the researchers have focused on developing prediction models implementing phenomenological and progressive damage approaches [5–10]. However, only the progressive damage approaches consider to some extent the damage mechanisms and accumulation process. The last decade, several researchers revisited the original idea proposed by Reifsneider and focused on understanding and unfolding the fatigue damage process. A common understanding has been established regarding the three states of damage development during fatigue of unidirectional, cross-ply and angle-ply composites [11–13];

- state I - damage initiation by formation of matrix cracking with numerous micro-cracks developed within the ply-level until saturation,
- state II – delamination onset, growth and mitigation to adjacent plies.

* Corresponding author.
E-mail address: d.zarouchas@tudelft.nl (D. Zarouchas).

https://doi.org/10.1016/j.jcomc.2021.100199
Received 12 September 2021; Received in revised form 22 October 2021; Accepted 28 October 2021
Available online 1 November 2021

- state III – damage progression in the matrix-fibre interface resulting in fibre debonding, fibre breakage, and pull-out, which eventually leads to the final failure.

Nevertheless, the precise damage accumulation sequence depends on the material properties of the composite's constituents, the exact layup, the defects induced during manufacturing, the loading profile and the environmental conditions in which the structure operates. Additionally, the inhomogeneous nature of the composite material and the stochastic activation of different damage mechanisms should also be taken into account making the damage process a very complex phenomenon to study.

Another structural health concern for any aircraft is foreign object impact events. Impacts can range from a local high-energy event such as a bird strike to distributed low-energy events, for instance during a hailstorm. Unlike metallic structures, composites often do not reveal any damage present. Incidents such as accidental tool drops during maintenance can create interlaminar damages that are invisible to the naked eye. In order to deal with this, a limit case is often taken into account, where a structure is designed to be able to sustain its loads with the presence of barely visible impact damage (BVID). Airworthiness regulations state that a structure containing BVID must still be able to sustain the loads seen, during the rest of the aircraft life. By definition BVID is hard to detect visually and therefore must be expected to stay unrepaired. AMC 20–29 (acceptable means of compliance) is a document by the European Union Aviation Safety Agency (EASA) covering compliance guidelines to aircraft certification specifications and it specifies five different categories of damage and the actions needed related to their severity [14].

In order to show that structures can sustain their required loads after damage, fatigue tests should be performed. Such fatigue tests are especially important for category 1 and 2 types of damage, since they need to sustain their loads for a prolonged period of time. Aside from the static and fatigue loads, the AMC document states that stiffness properties should not change significantly during fatigue testing. In addition, with the introduction of a 'slow-growth' approach by the Federal Aviation Administration (FAA) to the certification of composite structures [15], the regulations put emphasis on a structure being able to sustain loads after damage growth.

The importance of investigating the effects of such detrimental loading phenomena is evident. In addition, combinations of these phenomena can amplify the structural degradation. The combined effects of impact and other loadings have been studied by tension after impact (TAI), compression after impact (CAI) and fatigue after impact (FAI) [16–18]. Quasistatic CAI and compression-compression or compression-tension FAI have been studied the most, due to the propensity of composite materials to form interlaminar failures during an impact event, which typically reduces the compression strength significantly [19,20].

Because of the higher severity of compression loading after impact, tension loading is less researched and therefore less well understood. However, many areas on an aircraft that are primarily loaded in tension are also susceptible to impacts. For example, a wing's lower skin panel can be hit by runway debris during take-off or landing, or a tension-loaded fuselage section can be hit by hailstones or ground handling equipment. Kang and Kim have shown that impact indeed also has a detrimental effect on tension-tension fatigue [21]. Symons and Davies performed tension-compression fatigue tests ($R = -1$) on CFRP specimens with two types of impact loading: a 5 J impact creating BVID and a 10 J impact creating visible impact damage [22]. It was shown that doubling this impact energy reduced the fatigue life roughly by an order of magnitude. The coupons were taken out of the testing machines to be C-scanned at certain intervals, showing that the initial damage area due to the impact event does not increase significantly during fatigue testing. This was also observed by Swanson et al. [23]. The severity of the damage however did increase, as was observed visually in the form of cracks and local delamination buckles. In research performed by Koo et al., residual strength characteristics as well as residual fatigue life characteristics were found for specimens with impact damage [24]. Tests were performed with graphite/epoxy specimens with plain-woven prepreg plies. Impact energies of 5 to 23 J were used to determine residual static strength values. The fatigue tests were performed on specimens impacted with 5 J with a hemispherical impactor, which decreased the tensile strength to about 70% of its intact state. Cyclic testing was performed with a frequency of 5 Hz and a stress ratio of 0.1. It was concluded that the impact damage decreases the fatigue life of the specimens, while increasing the scattering range.

Tai et al. performed tension-tension fatigue tests after low energy impact of [0/45/90/−45]2 s carbon fibre epoxy laminates [25]. Ultrasonic C-scanning was used to show that the damaged area increased for larger impact energies, and indeed the damaged area grew during fatigue loading. Fatigue loading was performed at different maximum stress levels with a stress ratio of $R = 0.1$ and a frequency of 3 Hz. It was concluded that the impacted specimens not only exhibit reduced fatigue life as expected, but also have less scatter than the virgin specimens. Interestingly, the difference is larger for smaller maximum stress levels. This might be explained by the fact that at lower energies, failure is dominated by matrix cracking and delaminations, which are already present due to the impact event. At high stress levels on the other hand, the load is carried more by the fibres, which are largely unaffected by the low energy impact event. The stiffness change during the fatigue cycling was particularly interesting. During roughly the first 10^3 cycles the stiffness increased, after which it started decreasing up until failure. The authors explain that the stiffness is defined as the slope of the tangent of the stress/strain curve, but there is no explanation on how the strain data was measured. The initial increase in stiffness is explained by the possibility that the ±45 fibres might change orientation slightly upon loading, essentially straightening out and carrying more load with respect to the matrix. Lastly, the initial stiffness of the impacted specimens was lower than that of the intact specimens, and the stiffness reduction rate was higher.

It is apparent that these exercises increased our understanding of how impact damages a composite structure and how it affects its structural integrity. However, the impact is considered as an isolated loading scenario or as an event that occurs only at the beginning of the lifetime of a structure. This neglects for example the effects that any prior fatigue damage has on the damage response of an impact event. A projectile with a certain energy that would normally create BVID may create a different damage state with other damage already present. No literature was found on the effects of impact events during fatigue loading and we believe that it is a research topic worth to explore.

Narrowing down the broad problem description above, the purpose of this paper is to experimentally investigate the effects of combined impact and fatigue loading while fatigue damage is already present. A novel experimental set-up was designed where a mechanical testing machine was used for cyclic loading, with a gas gun positioned next to it so that specimens could be impacted in-situ. Digital image correlation (DIC) was used to track the strain response of each specimen during testing, which was also used as a criterion to decide the moment of impact. In addition, acoustic emission (AE) measurements were performed to gain additional knowledge on damage accumulation during testing. Some tests were not run until failure in order to be inspected using ultrasonic C-scanning to map the delaminated areas.

The remainder of the paper is organized as follows: Section 2 discusses and motivates the decisions made for the experimental campaign, i.e. the selection of the location and time to impact, the type of the projectile, the energy level. Section 3 presents the composite material used on this study and the experimental procedure while Section 4 presents and discusses the results. The conclusions are given in Section 5, along with a discussion for future work.

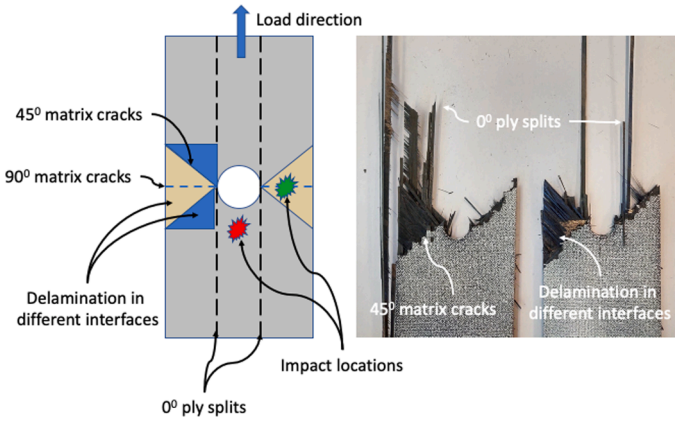

Fig. 1. A schematic of damage pattern of an open-hole quasi-isotropic lay-up subjected to tension-tension fatigue loading.

2. Design of the experimental campaign

The objective of this paper is to experimentally investigate the effects of the timing of an impact event on the fatigue life and damage patterns on carbon fibre reinforced polymers, commonly used in aviation industry. For a given lay-up and geometry of a structure, there are several experimental parameters that should be considered for the execution of the tests;

- fatigue testing parameters, i.e. loading ratio, frequency, maximum load
- impact location
- time of impact and consequently damage state of the structure
- stress level within the fatigue cycle
- energy of impact, geometry, shape and material of the impactor

It is well known that the fatigue damage accumulation process and subsequently the fatigue life depends on the fatigue testing parameters, i.e. loading ratio, frequency, maximum load level, for example see [26,27]. It is out of the scope of this paper to review the effect of these parameters and our selection had a practical background concerning the time execution. The parameters are presented in the next section.

The experimental campaign is tailored for open-hole specimens where the location of impact, in respect to the notch, can influence the damage pattern, damage propagation and subsequently the fatigue life. Notched composite structures have been extensively studied the last four decades; the studies focused on analysing the size effect of the notch on the strength and fatigue life, assessing the progression of damage and measuring residual properties, i.e. strength and stiffness [28–30]. The open-hole specimen configuration is selected in this study as a range of effects appear, i.e. stress concentrations and manufacturing defects due to machining that represent better the reality and are not observed in unnotched specimens [31]. At the same time, due to high stress concentrations, the damage will initiate at the notch and propagate in a confined area (the extension and damage growth depend on the material, lay-up configuration, ration between the width of the specimen and the hole diameter [31]) offering an opportunity to study the effect of impact at different location in respect to the damage area.

Fig. 1 presents a schematic of a typical fatigue damage pattern for a quasi-isotropic lay-up of an open hole CFRP specimen subjected to tension-tension fatigue. Transverse matrix cracks initiate at the 90 ° layers (blue dash line, Fig. 1), occurring at the hole edges, and propagate towards the specimen's edges. In parallel, off-axis matrix cracks occur at 45° (blue line, Fig. 1) and they introduce delaminations at the adjacent interfaces (yellow and blue triangles, Fig. 1) close to the hole, which propagate towards the specimen's edges and along its length. Finally, fibre splits initiate at the hole edges of the on-axis ply (black dash line, Fig. 1) and propagate along the specimen's length. The last damage mechanism creates a stress-free zone under the hole.

In our previous study, we selected the location of impact within the damage propagation zone (green spot, Fig. 1), as the goal was to accelerate the damage progression and reduce the fatigue life of the specimens [32]. It was found that the later the specimen was impacted the shorter its fatigue life was demonstrating our hypothesis that the timing of impact can influence the fatigue life. However, in order to test this hypothesis for other impact locations, for this study we selected a spot outside the damage propagation zone (red spot, Fig. 1).

In order to be able to compare and build confidence about the results, the timing of the impact should be carefully selected. In the previous study, we impacted three specimens at three different predefined fatigue cycles between 0–20k cycles, neglecting the damage state of each specimen. However, despite the fact that the specimens were nominal identical and were subjected to the same loading conditions, the fatigue damage accumulation process is most likely different for each specimen meaning that the damage state as a function of fatigue cycles differs from specimen to specimen. Taking into account that, in this study we propose a strain increase criterion in order to select the timing of impact; it is expected that the increase of strain during the fatigue is a better indicator of the damage state than simply the number of cycles a specimen has gone through and in order to achieve that real-time monitoring of the strain is needed. This is further explained in the next section.

Another important parameter is the stress level that the specimen is subjected to, at the time of impact. The literature is limited to pre-stressed structures subjected to impact and only for static loads. Johnson et al. examined the damage tolerance of pre-stressed composite panels under impact within the framework of LIBCOS project [33,34]. For the case of the tensile pre-stressed conditions, the authors found that the low pre-stress levels had no detrimental effect on the residual strength. In the current study, taking into account some implications of the experimental procedure, it was chosen to interrupt the fatigue test, pre-stress the specimen at the mean load value of the tensile fatigue loading range and impact. In this way, we could be consistent and create a systematic data base for analysis.

The energy of impact, geometry and material type of the impactor play a role on the severity and type of the induced damage. Regarding the energy of impact, preliminary impact tests took place in order to determine the energy level required in order to introduce BVID and it was found that for the specific composite material and lay-up configuration, energy levels up to 12 J can create BVID, so 10 J was selected. Furthermore, Shat et al. discussed in their review paper that for a given shape of impactor, by decreasing the diameter the impact resistance of the composite structures decreases and more damage occurs for the same energy [35]. Regarding the shape, the impactor with the larger contact area introduces the largest damage. Finally, a material with higher stiffness will transfer to the composite structure a bigger portion of its kinetic energy just before the impact.

3. Material & experimental set-up

3.1. Material

The specimens used in this testing campaign are made from carbon prepreg Toray specification BMS 8–276 and type 35 – class 10. Eight plies of unidirectional (UD) prepreg were used in a quasi-isotropic pattern, with a ply of plain woven (PW) (0/90) prepreg on either side. The nominal cured thicknesses of the UD plies and the woven plies are 0.190 mm and 0.218 mm respectively. The layup used is $[(0/90)_F/45/90/-45/0]s$, which has a total cured thickness of about 2 mm. For further information about the manufacturing process, the reader should refer to [36].

Four laminates were roughly cut using a Carat liquid-cooled diamond saw, followed by precise cutting using a Proth Industrial liquid-cooled saw. Each laminate produced 10 specimens. Because of the

Table 1
Results of the static tests.

Specimen ID	UTS (kN)	Failure strain (%)	Test machine control
16	43.6	1.22	1 mm/min
20	46.5	1.25	1 mm/min
33	44.8	1.22	1 mm/min
48	42.0	1.17	1 mm/min

possibility of variation between the four panels, care was taken to use random specimens for each test series. An ID was given to each specimen, see the first column of Tables 1 and 2, that was a number starting from 10 up to 49, for example the specimen 38 is the 8th specimen from the 3rd laminate.

The specimens had 400 × 45 mm dimension, with a 10 mm central hole. The outer 50 mm on either side of the specimen was used to clamp in the hydraulic grips of the fatigue machine, so the distance between

Table 2
Results of the experimental campaign.

Specimen ID.	Paused at strain increase %	Paused at fatigue cycle [10^3]	C-Scan at fatigue cycle [10^3]	Impact (10 J) at fatigue cycle [10^3]	Fatigue life [10^3]	Test condition
46	No pause	No pause	No	No	29.4	1
10	No pause	No pause	No	No	37.7	1
18	No pause	No pause	No	No	37.0	1
43	0	0	No	No	54.3	2
14	0	0	No	No	76.3	2
39	0	0	No	No	114.6	2
42	0	0	No	Yes	8.8	3
30	0	0	No	Yes	10.9	3
25	0	0	No	Yes	28.3	3
22	14	13.7	No	No	90.2	4
34	14	6.1	No	No	23.2	4
45	14	19.7	No	No	87.2	4
24	14	13.1	No	Yes	114.2	5
41	14	10.1	No	Yes	36.9	5
44	14	17.1	No	Yes	50.4	5
23	20	41.2	No	No	72.6	6
11	20	16.2	No	No	29.5	6
31	20	10.6	No	No	23.0	6
47	20	34.7	No	Yes	81.4	7
17	20	36.3	No	Yes	49.4	7
38	20	16.7	No	Yes	25.9	7
12	0	0	Yes, at 0 cycles	No	Terminated	8
49	0	0	Yes, at 0 cycles	Yes	Terminated	8
19	0	0	Yes, at 0 cycles	Yes	Terminated	8
29	0	18.0 cycles (20% strain increase)	Yes, at 18.0 cycles	No	Terminated	8
21	0	7.3 cycles (20% strain increase)	Yes, at 7.3 cycles	Yes, at 0 cycles	Terminated	8
15	14	17.2	Yes, at 17.2 cycles	No	Terminated	8
28	14	15.2	Yes, at 15.2 cycles	Yes, at 15.2 cycles	Terminated	8
40	14	28.5 (20% strain increase)	Yes, at 28.5 cycles	Yes, at 28.5 cycles	Terminated	8
37	20	22.3 cycles	Yes, at 22.3 cycles	No	Terminated	8
32	20	33.2 cycles	Yes, at 33.2 cycles	Yes, at 33.2 cycles	Terminated	8

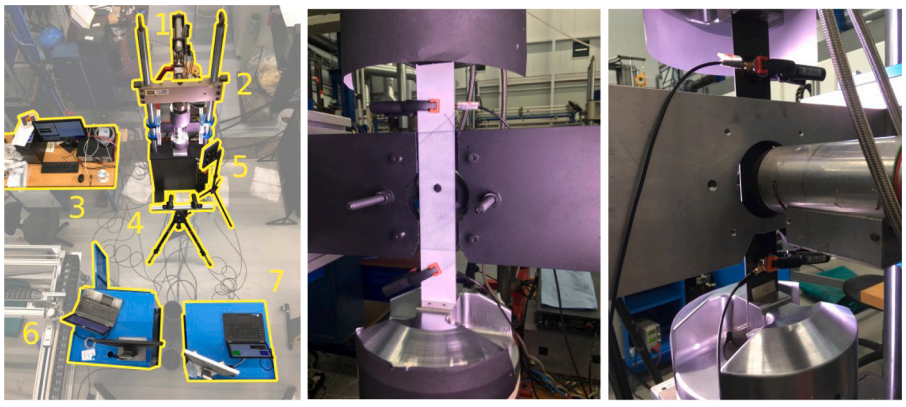

(A) (B) (C)

Fig. 2. A. The overview of the experimental set-up (1) Gas gun (2) Servo-hydraulic test machine (3)Test machine controller & interface (4) DIC cameras (5) Light source for cameras (6) DIC data acquisition (7) AE data acquisition. 2.B. The front of the specimen clamped into the testing machine. 2.C. The rear of the specimen clamped into the testing machine.

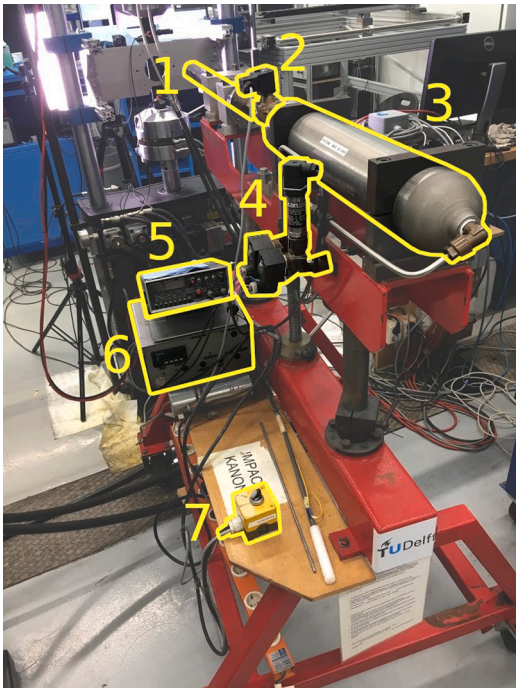

Fig. 3. The impact gas gun with (1) barrel (2) trigger valve (3) air pressure tank (4) pressure sensor, fill valve and empty valve (5) velocity measurement display (6) control unit and (7) trigger switch.

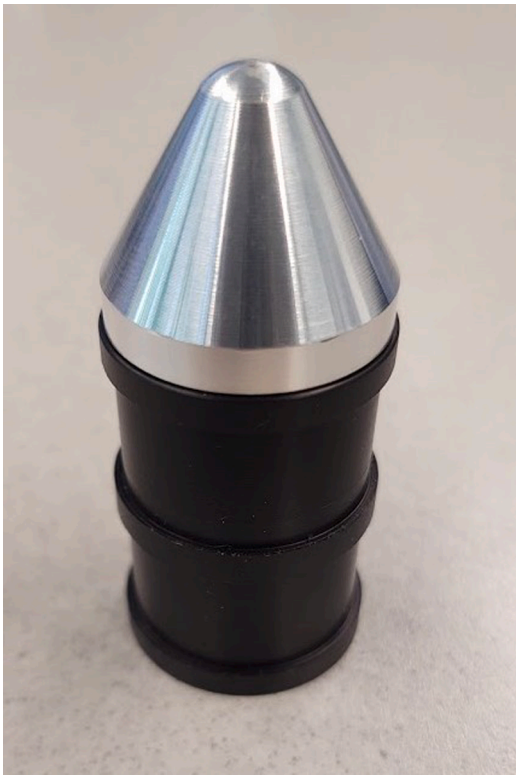

Fig. 4. The aluminium projectile screwed into a POM rear section.

the grips that was actually loaded was 300 mm. Paper end tabs were glued to these end sections to create more friction between the specimen and the clamps.

3.2. Experimental set-up

An overview of the test area is shown in Fig. 2A, with important pieces of equipment numbered and explained, while Figs. 2B and 2C present the front and rear of the specimen clamped into the testing machine.

Note the safety device that is painted black (Fig. 2B.) to avoid excessive reflections from the Digital Image Correlation (DIC) light source entering the cameras. Black screws are used to cover holes which would otherwise reflect light on their inner thread, thus overexposing the cameras. Black paper is taped onto the upper and lower grip heads on the test machine for further glare reduction. Two black clamps can be seen on the specimen. These are each situated 100 mm from the central hole and serve to clamp the Acoustic Emission (AE) sensors to the back of the specimen.

The gas gun is shown in Fig. 3 with the various components highlighted and explained. The gas gun was aimed at the rear side of the specimen, to avoid any interference with the DIC setup. Before starting any fatigue test, a bullet was loaded from the front of the barrel, pushing it back until it reached a narrow section. The required air pressure was set on the control unit (6). When the fatigue test was interrupted in order to impact, the tank (3) was filled using a tube from an external compressed air source. The device was then triggered using a switch (7), opening the trigger valve (2), releasing the gas and thus shooting the impactor. The velocity could then be calculated from the time difference measured by two sensors, shown on the display (5).

All tests were performed on a servo-hydraulic MTS fatigue machine with capacity of 100 kN. First four quasi-static tensile tests were performed to measure the ultimate tensile strength (UTS) and global failure strains as shown in Table 1. These tests were displacement controlled, with a speed of 1 mm/min.

For cyclic load testing, all tests were performed with the same fatigue parameters. The load was applied with a frequency of 10 Hz, $R = 0.1$ and with a peak load of 80% of the UTS load, 35.4 kN.

It is recognized with such a high maximum fatigue load, the off-axis plies will already be damaged within the first loading cycle. This became immediately clear due to audible and visible cracking upon first loading. Nevertheless, such high maximum loads were deemed inevitable when testing until failure due to time constraints.

For the combined loading tests, the impact event on a specimen has to occur somewhere during the fatigue program. It is desirable to leave the specimen in the machine for this, as taking it out and clamping it back in again will create slight differences in boundary conditions. Also, it would mean that the specimen will be fully unloaded for a while, and it will take longer before the cyclic loading program can be continued. In order to resemble a situation as close as possible to a true impact during cyclic loading event, the fatigue program was interrupted and the specimens held at a constant load. This constant load was necessary to ensure that every impact occurs at the same preload. Moreover, the AE sensors could be damaged by an aggressive event such as impact, so they had to be removed beforehand.

To serve as impactors, custom bullets were produced with an aluminium tip screwed into a POM (Polyoxymethylene) rear section, see Fig. 4. The tip is hemispherical with a radius of 5 mm and the plastic rear section acts mainly to seal the gap between the barrel and the bullet. A secondary function is to ensure the centre of mass of the impactor lies in front of the centre of pressure, which guarantees stable flight. The mass of a single bullet was 30.7 g. The variation in mass between the bullets was less than 0.1 g, not enough to cause significant differences in the impact energy.

A device was used to measure the travel time between two sensors as the bullet left the barrel. With this travel time, the bullet velocity was calculated. The impact energy was chosen to be 10 J for all specimens to be impacted. In order to achieve this, an air pressure of 1.45 bar was used in the gun, giving the bullet a velocity of 25.5 m/s and since the end of the barrel was positioned very close to the specimen, deceleration due

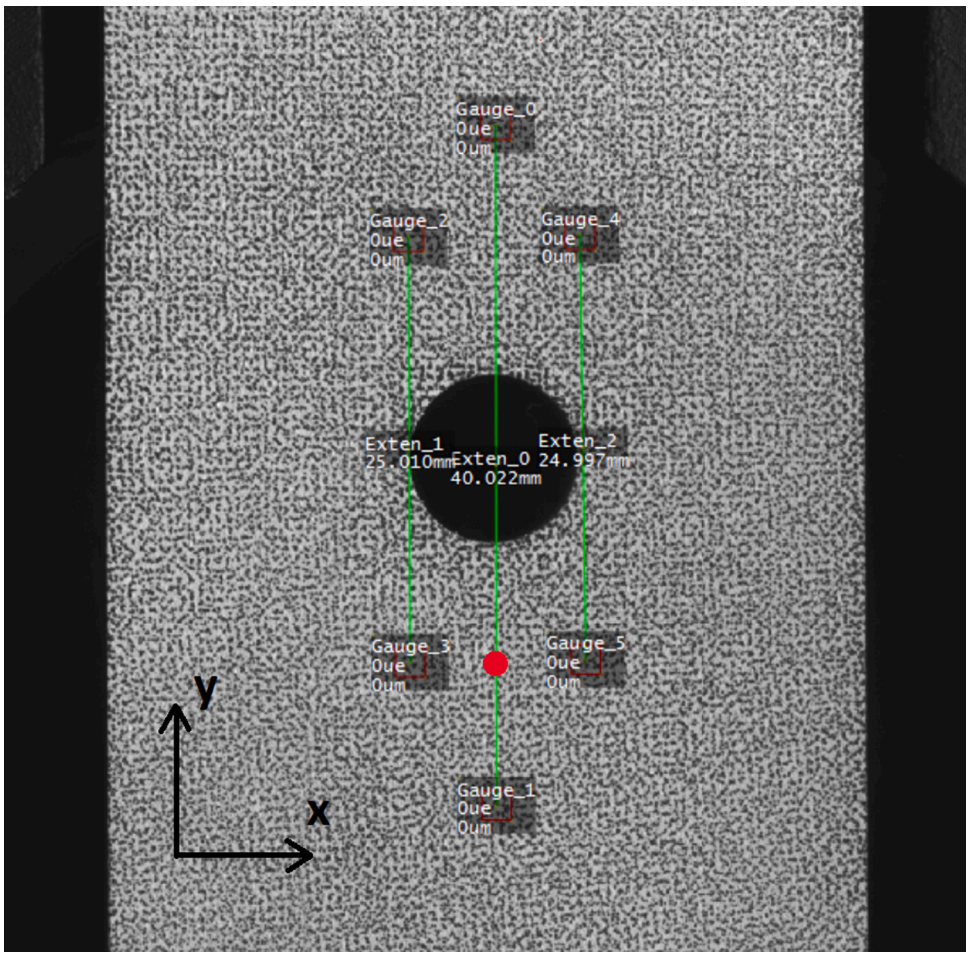

Fig. 5. Virtual extensometer placement (green lines) and a typical impact location (red dot).

to aerodynamic drag is neglected. The impact gun was aimed such that the bullet would hit the specimen 5 mm below the hole edge.

Different types of measuring equipment were used. A DIC system measured the surface deformations and strains. Two Flir 5 MP cameras with a 50 mm lens were used, in a distance of about 800 mm from the specimen. Since the all the specimens had a central 10 mm hole, it was expected that this was the primary area where damage would occur and propagate. The field of view of the cameras was about 140 mm along the specimen, with the full specimen width within the frame. The VIC-Gauge software was used in order to track the strain response during fatigue loading. Three virtual extensometers were placed across the hole, all in vertical-orientation, direction of the load, as shown in Fig. 5. The typical impact location is shown as well, in the form of a red dot below the hole. The central extensometer has a length of 40 mm, with the two outer extensometers having lengths of 25 mm. Care was taken to ensure that the extensometers were positioned parallel to the longitudinal specimen axis, and that the variation in extensometer length was low. This variation was typically below 0.1 mm. By taking the average value of the tensile strains measured by the extensometers, the strain response was tracked in real-time during fatigue cycling. At the same time, the Flir cameras recorded images every 500 cycles at the minimum and maximum load level of the fatigue loading range. These images were used for post-processing to calculate the full field strain fields.

The real-time strain measurement allowed us to set a strain-based criterion for selecting a common threshold for the timing of the impact. Three strain increase values 0%, 14% and 20% were selected as the moment to perform the impact. The strain increase refers to the initial strain measurement at the beginning of each test. The selection of these three values was based on the strain analysis from the fatigue tests, see Fig. 7a. The 0% strain increase refers to the tests for which the specimens were impacted before the fatigue loading. The 14% value refer to the moment after the initial rapid strain increase while the 20% value refer to the half-way duration for the slow growth part.

As long as a strain increase of 14% or 20% was recorded by the VIC-gauge software, the fatigue test was interrupted, the specimen was held at the mean value of the fatigue load range. This procedure was common for all specimens, with and without impact, so as to ensure the same testing conditions. The time of interruption was 9.5 min, which was the time needed to prepare and execute the impact.

Fig. 6 presents a schematic of the testing procedures. The experimental campaign consists of 8 testing conditions. The first 7 conditions refer to the fatigue tests that run until the specimen fails, while the 8th condition refers to the specimens for which the fatigue test was interrupted in order to perform a C-scan. More specifically, test condition 1 is the continuous fatigue test until failure, test condition 2 refers to the pause at 0% strain increase and then fatigue until failure, test condition 3 refers to the pause at 0% strain, then impact and afterwards fatigue until failure. Accordingly test condition 4 and 5 refer to the pause at 14% strain increase without and with impact while test conditions 6 and 7 refer to the pause at 20% strain increase without and with impact.

The accuracy of the DIC setup used was checked for each specimen by taking several images before any load was applied. Comparing these images in post-processing shows the noise of the system. As an example, Fig. 7 shows the surface strain error in longitudinal direction of specimen 23. The noise error is between −93 and 100 microstrain, roughly an error of 200 microstrain in total. With a first measured strain value typically in the order of 10′000 microstrain, a 2% error is deemed acceptable. The other specimens checked for accuracy had very similar

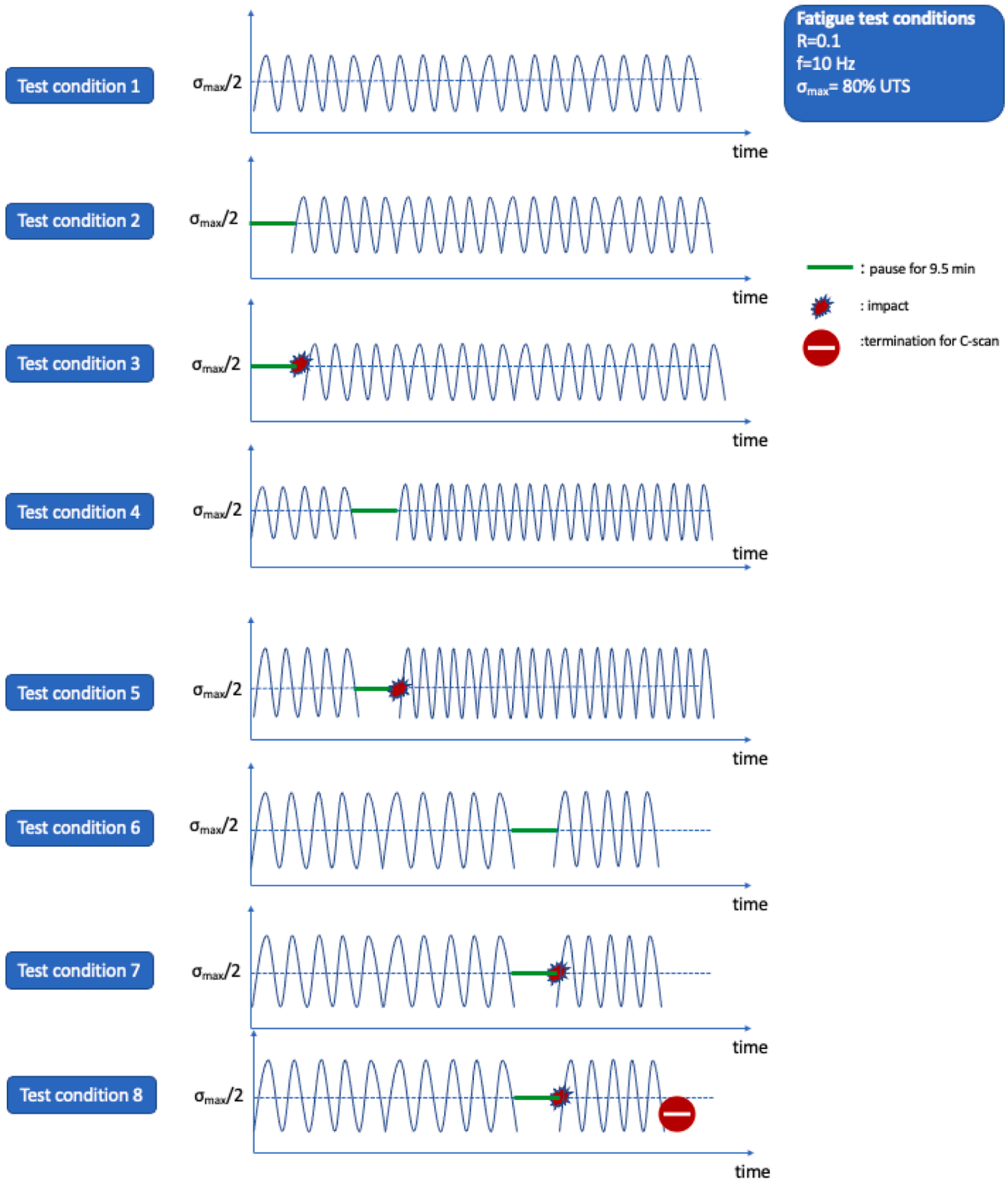

Fig. 6. A schematic of the experimental procedure with the 8 test conditions.

error levels.

Furthermore, an AMSY-6 AE measurement setup from Vallen Systeme GmbH was used. Two Vallen VS900-M passive AE sensors were used with a frequency range of 100–900 kHz. The sensors were clamped onto the specimens with coupling fluid to allow for good transmission of acoustic waves. Each sensor was wired to a preamplifier with a gain of 34 dB, before the signals were passed onto a data acquisition device. The system was linked to the MTS machine, so the force and displacement that the machine measures were stored in the AE data as well.

In addition to the specimens that were tested to failure, 10 specimens were tested up to a certain point, after which they were C-scanned. The images are black and white, without differentiation between the various plies. While the resolution is fairly low, about 0.55 mm per pixel, the contrast is good, and a clear boundary between the damaged and intact

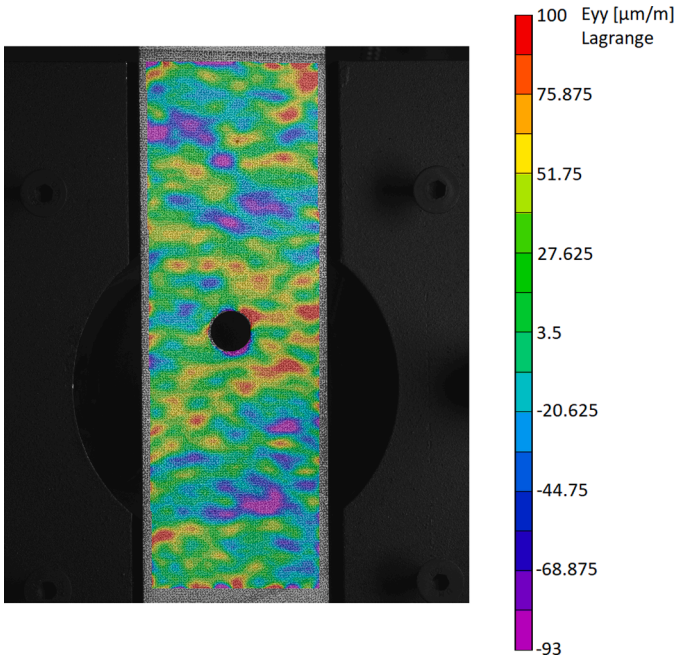

Fig. 7. A typical DIC error measurement in microstrain.

area is seen.

4. Results & discussion

This section presents the experimental results and it is divided into four parts. The first part discusses the fatigue tests without any impact, the second part compares the fatigue tests with and without impact before the fatigue (0% strain increase), while the third and fourth parts compare the fatigue tests with and without impact for 14% and 20% strain increase.

Table 2 summarizes the experimental effort of this study by presenting the number of fatigue tests, the fatigue life and the loading conditions. In total 31 fatigue tests were performed, from which 21 specimens were loaded until failure while the tests of the remaining 10 specimens were terminated at the 3 predefined strain increase level for C-scan analysis.

It should be reiterated that when strain percentages are discussed, an increase of longitudinal ε_{yy} surface strain with respect to the first measured value of a specimen is meant. Throughout this section, graphs are shown with the strain increase of specimens over their fatigue life. These are always normalized with respect to the first strain measurement before the start of the fatigue cycle. This normalisation and comparison between different specimens is deemed acceptable since the first measured values were very similar. The average value encountered was 10,060 microstrain (about 1.01%) with a standard deviation of 220 microstrain. Note that the estimated measurement error is 200 microstrain as presented in the previous section.

4.1. Fatigue tests

Fig. 8a shows the strain increase of the specimens as a function of the fatigue life. Although there is significant scatter related to the fatigue life, the strain increase at the moment of failure is similar for all specimens and it ranges between 40% and 50%. Furthermore, it can be observed that the strain curves follow an S-shape, where initial strain increases quickly until about 10–12%, after which the increase slows down to an almost linear path. This part consumes most of the fatigue life of the specimens. After about 25–30% increase, it starts to speed up again and critical failure is imminent.

Three samples were not paused (pure fatigue test), and the other 9 were paused at 0%, 14% and 20% strain thresholds respectively. A difference is observed between the mean fatigue lives of each test type, see Table 2. The fatigue life of the samples paused immediately at the start (0% strain increase) is on average more than twice as long as that of the uninterrupted specimens. If the interruption indeed has an effect, it is likely that any influence of this pause has less of an effect the later a specimen is paused. This seems to be true, as the mean fatigue life of the

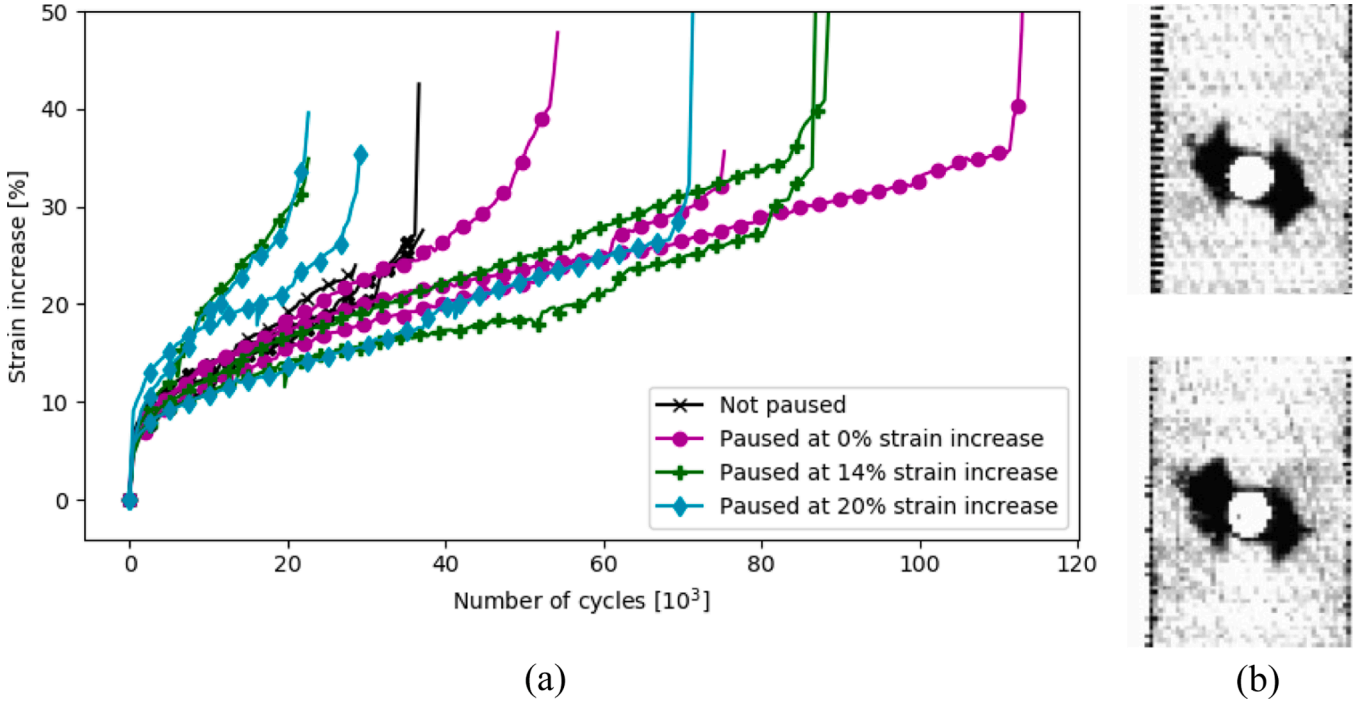

Fig. 8. (a) The strain curves for all the specimens subjected to fatigue and (b) C-scan images for specimens 29 – paused at 0% strain increase and scanned at 20% strain increase (upper) and 37 – paused and scanned at 20% strain increase (lower).

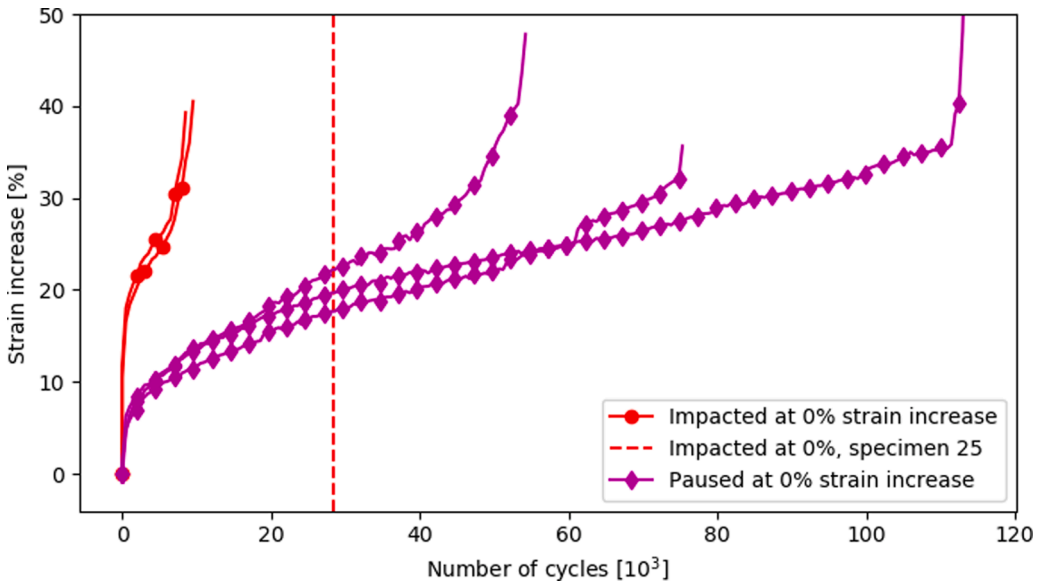

Fig. 9. The strain curves for all the specimens paused at 0%.

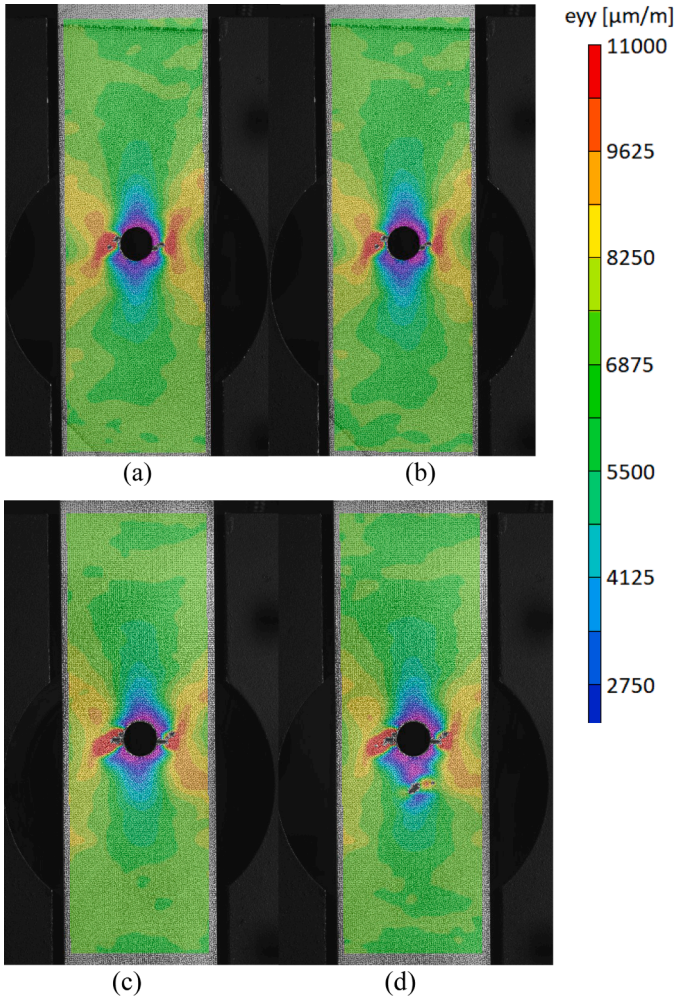

Fig. 10. Longitudinal surface e_{yy} strain for samples paused (top, specimen 14) and impacted (bottom, specimen 30) after 0% longitudinal strain increase.

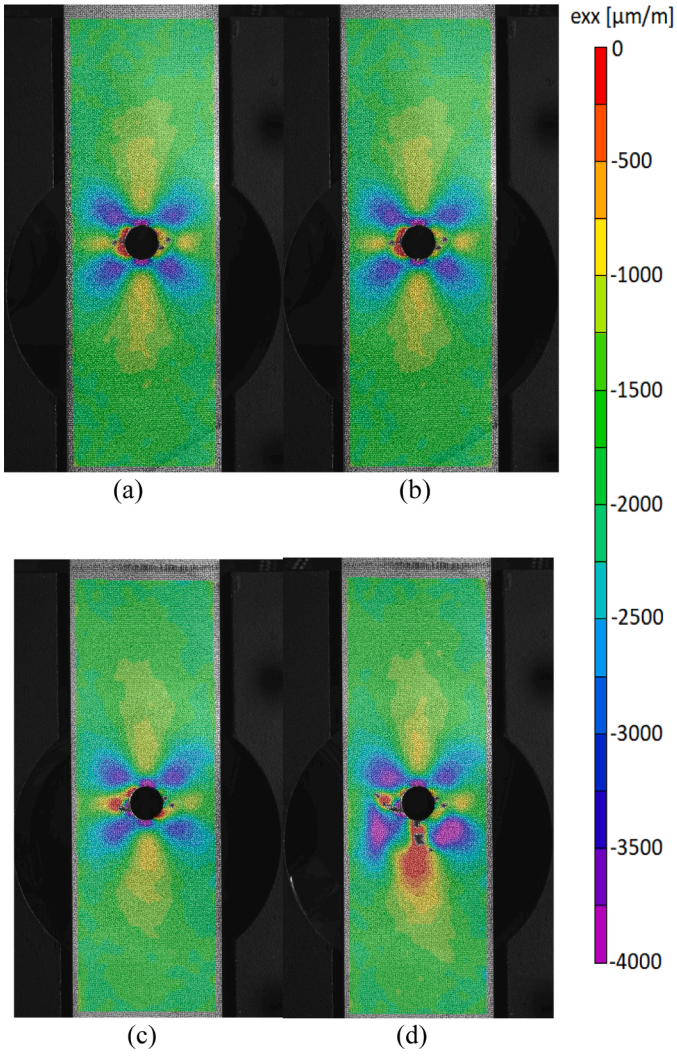

Fig. 11. Transverse surface e_{xx} strain for samples paused (top, specimen 14) and impacted (bottom, specimen 30) after 0% longitudinal strain increase.

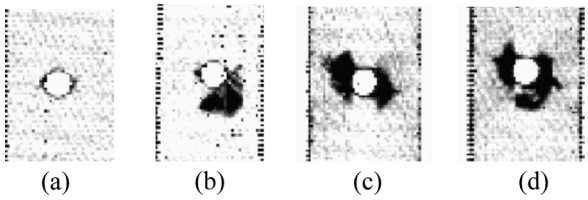

Fig. 12. C-scan images for specimens 12 – paused and scanned at 0% strain increase (a), 49 – paused, impacted and scanned at 0% strain increase (b), 29 – paused at 0% strain increase and scanned at 20% strain increase (c) and 21-paused and impacted at 0% strain increase and scanned at 20% strain increase (d).

20% samples is shorter than that of the 14% samples, which in turn has a shorter fatigue life than the 0% samples.

Fig. 8b shows two specimens that were loaded up to a strain increase of 20%. Specimen 29 was paused at 0% directly at the start, after which it was loaded until the 20% threshold was reached. Specimen 37 was first fatigued until 20%, after which it was paused and stopped. Both images look very similar, indicating that the moment at which a fatigue program is interrupted does not have a severe effect on the damage area for specimens subjected to fatigue loading only. Furthermore, during the pause AE did not record any hits, so it reasonable to assume that no damage occurred during this time.

4.2. *Paused at 0% strain increase*

Fig. 9 shows the difference in strain increase for the 0% samples.

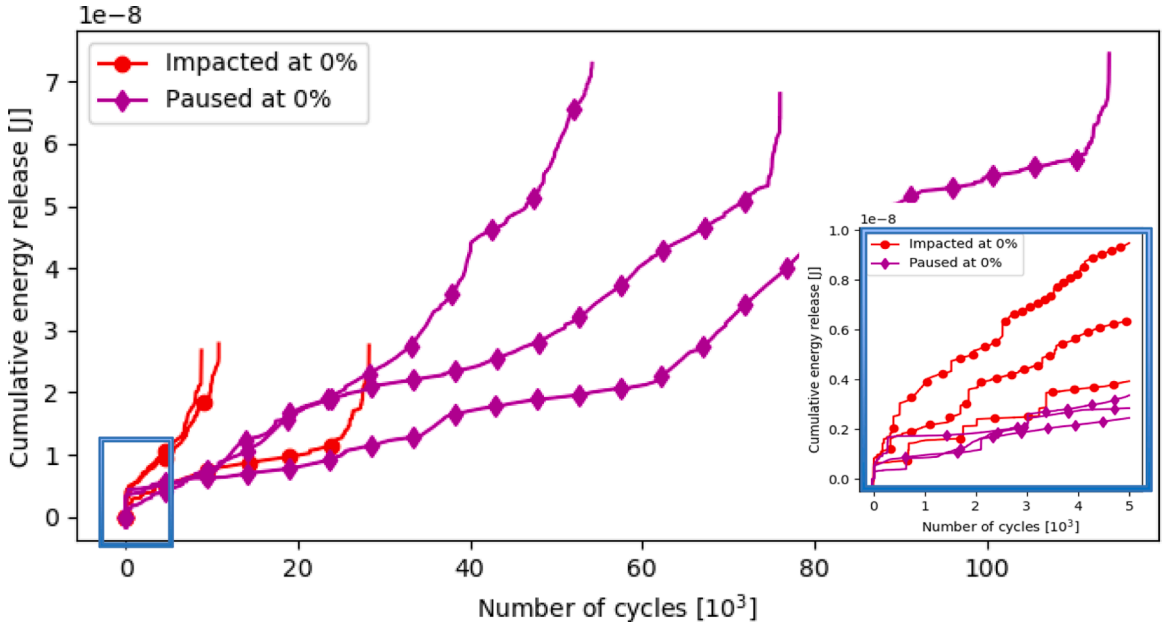

Fig. 13. Cumulative energy plots of samples paused at 0% with a highlight between 0 and 5000 cycles.

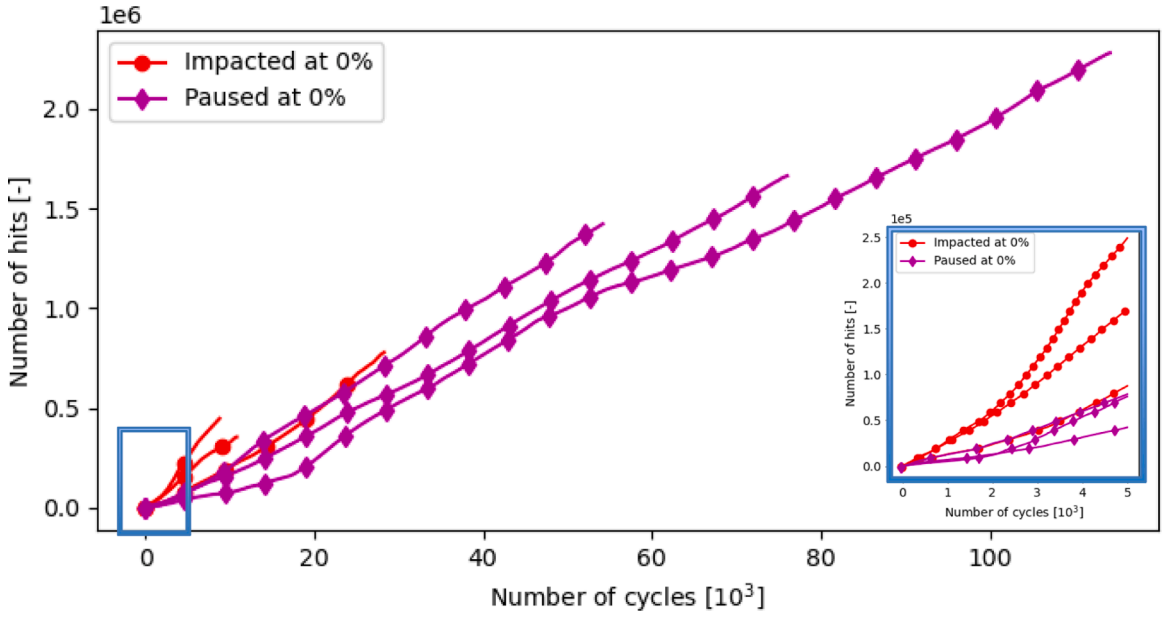

Fig. 14. Cumulative number of hits of samples paused at 0% with a highlight between 0 and 5000 cycles.

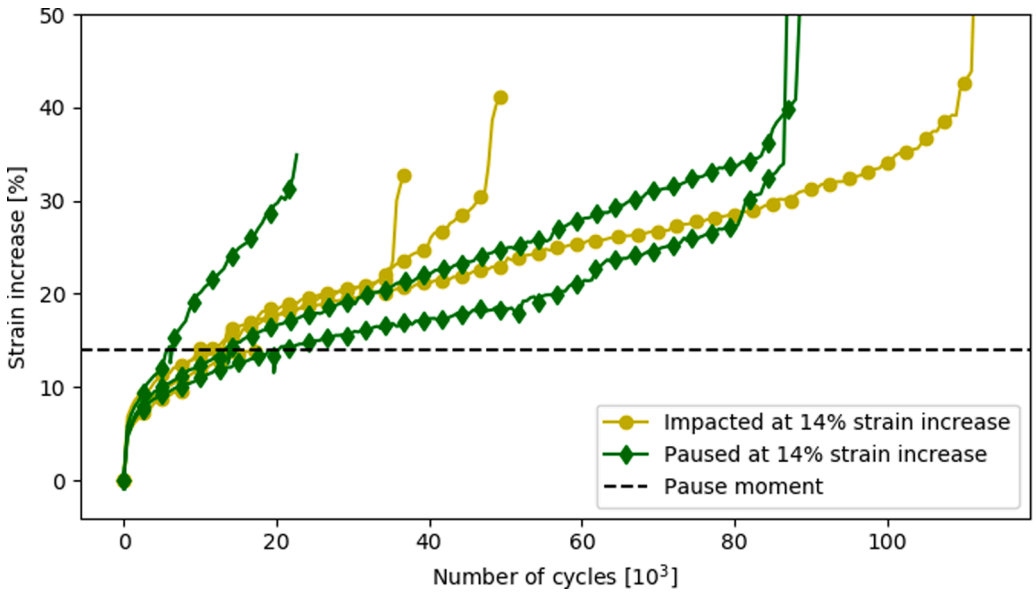

Fig. 15. The strain curves for all the specimens paused at 14%.

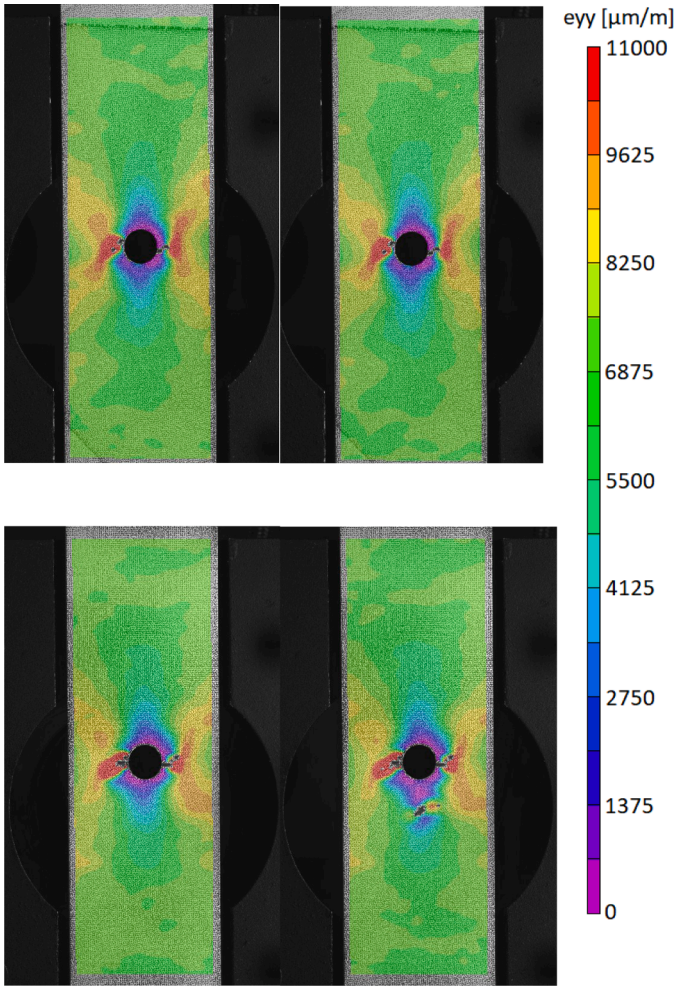

Fig. 16. Longitudinal surface e_{yy} strain for samples paused (top, specimen 45) and impacted (bottom, specimen 41) after 14% longitudinal strain increase.

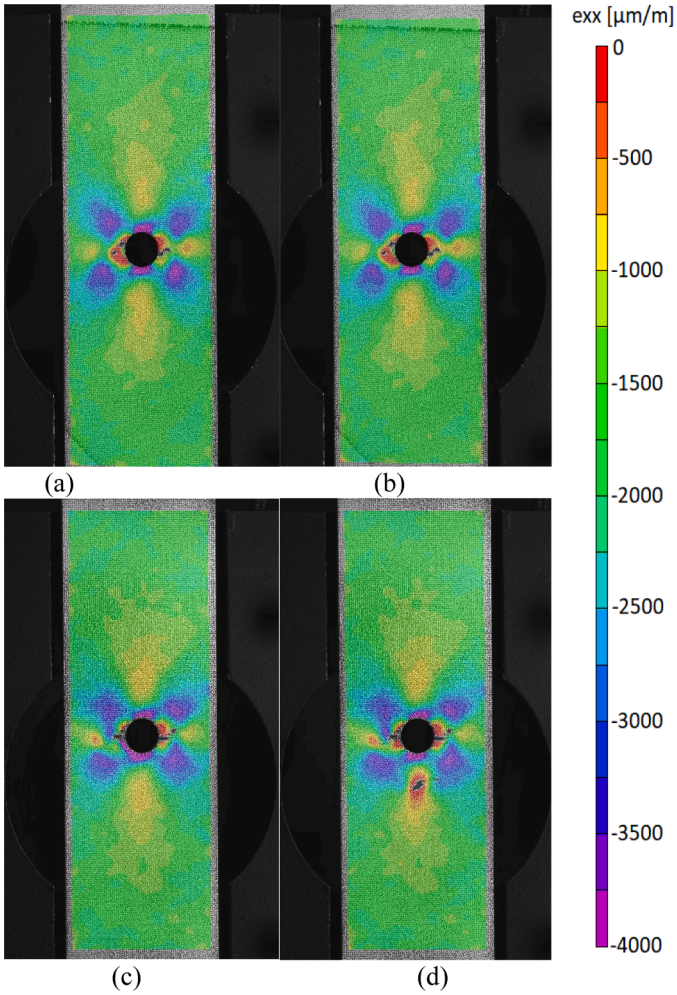

Fig. 17. Transverse surface e_{xx} strain for samples paused (top, specimen 45) and impacted (bottom, specimen 41) after 14% longitudinal strain increase.

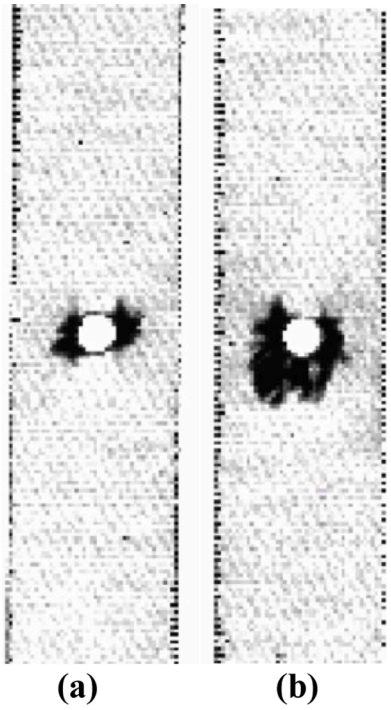

Fig. 18. C-scan images for specimens 15 – paused and scanned at 14% strain increase (a) and 28 paused, impacted and scanned at 14% strain increase (b).

Note that some paint chipped off from specimen 25 during the impact which compromised one of the virtual extensometers. No local strain data was therefore collected, so a dashed line is drawn at the fatigue life of this specimen. It is clear from the graph that the impacted specimens accumulate damage faster than the specimens that are merely paused. There is however not much difference in final failure strain values, it is just that the slow growth part is skipped. One could speculate that the impact caused delamination that entered the damage propagation zone and it drastically accelerated the fatigue failure. This hypothesis is supported by the DIC and C-Scan analysis.

Fig. 10 shows the longitudinal ε_{yy} surface strain field of two specimens as measured by the DIC setup. The top two images (a,b) show specimen 14 right before and after pause (without impact), and the bottom images (c,d) show specimen 30 right before and after impact. Note that the first images already show some cracking next to the hole. This is because the specimen needs to be loaded to the maximum fatigue load in order to take a DIC image pair. The bottom images clearly show the point of impact below the hole; some paint chipped off and a low stress region appears. An increase in damage is seen next to the hole, primarily to the left side. The visible crack increased in length and the stress distribution changed after impact.

Fig. 11 shows the transverse surface ε_{xx} strain fields of a paused and impacted specimen. Again, the paused specimen on the top does not show any difference. The impacted specimen however shows a significantly different strain field. The area on the bottom edge of the hole is relieved of its high compressive strain, and the blue/purple area with high compressive strain to the bottom left of the hole did not only increase after impact, but it changed shape as well. The triangular shape with one edge along the length of the specimen and the other two edges on a +/- 45 ° angle likely indicate a delaminated area underneath.

Furthermore, C-scans of four different specimens are presented in Fig. 12. Fig. 12a shows specimen 12 after only the pause moment. There is only a bit of damage observed on the two sides of the hole, as the result of the single loading cycle that is needed to take the DIC pictures and it can be related to the initiation of transverse and off-axis matrix cracks, see Fig. 10a,b. Fig. 12b shows specimen 49 that was impacted after the pause. A clear triangular damaged area is located below the hole whereas the right side of the hole is also damaged. This is in line with the observation made by DIC analysis, see Fig. 11c,d. Fig. 12c,d show the damaged area for specimen 29 that is not impacted and reached 20% increase of strain and for specimen 21 that is impacted at 0% and reached 20% increase of strain. The damaged areas left and right of the hole (fatigue damage propagation zone) are similar, the main difference is the damage area below the hole due to the impact. However, specimen 29 needs 18k cycles to reach the 20% strain increase while specimen 21 reaches 20% in 7.3k cycles, see Table 2, confirming that the impact accelerated the damage propagation and led the specimens with impact to fail much faster.

Fig. 13. shows the cumulative AE energy released. The sensors were removed for during impact in order to avoid damaging them, so the energy release due to impact was not measured. Furthermore, the cumulative energy for the period between 0 and 5000 cycles is highlighted where more than 30% of the total cumulative energy was released for the impacted specimens while for the specimens without impact the energy release was less than 5% of the total cumulative energy. A similar

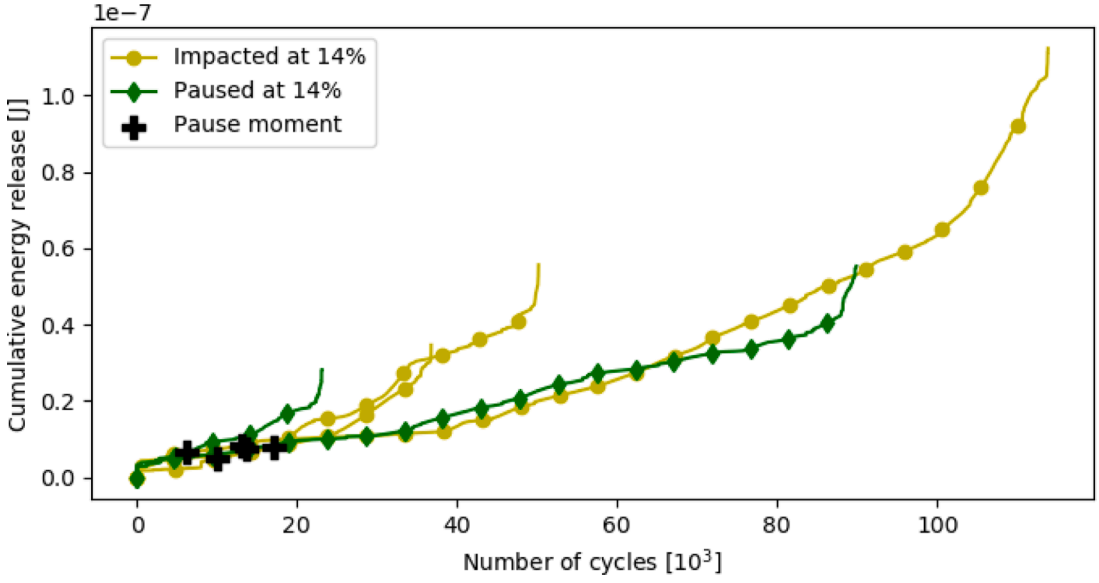

Fig. 19. Cumulative energy plots of specimens paused at 14%.

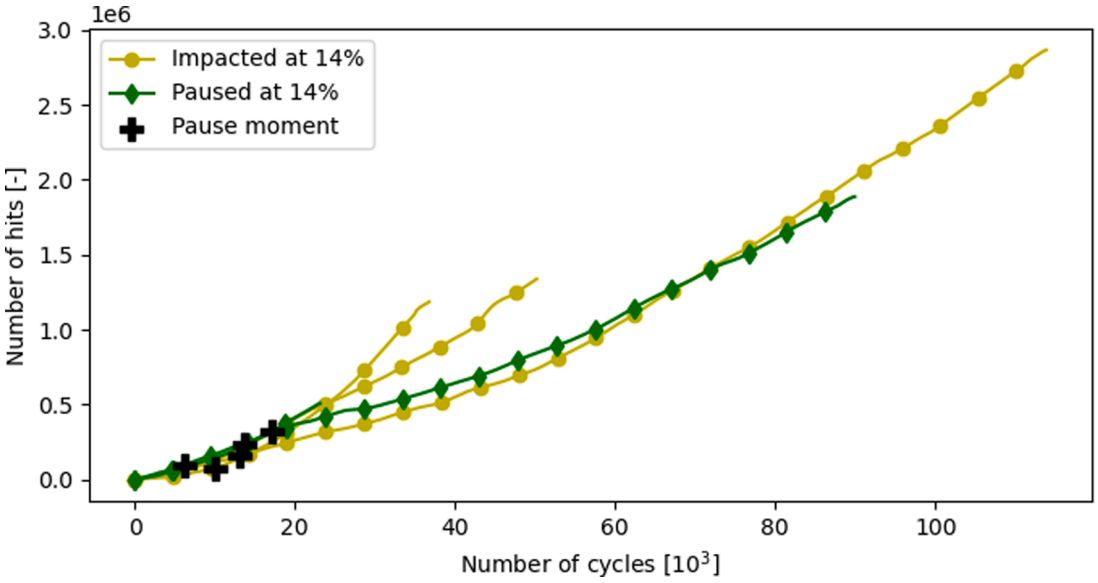

Fig. 20. Cumulative number of hits plots of specimens paused at 14%.

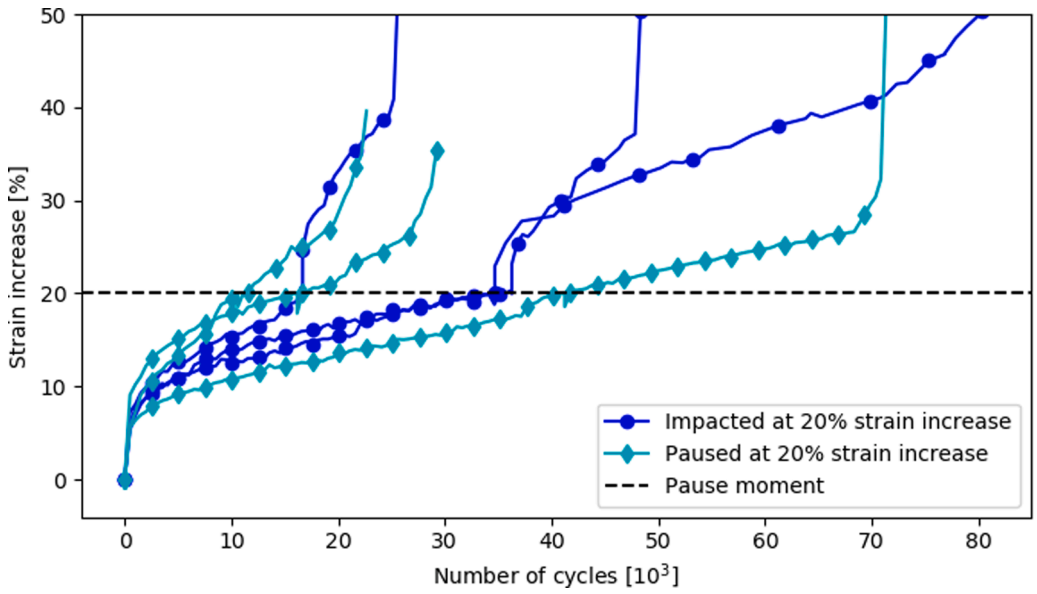

Fig. 21. The strain curves for all the specimens paused at 20%.

analysis stands for the number of hits as presented in Fig. 14. In line with DIC and C-Scan, the AE results also confirm that the impact accelerated the damage process.

4.3. *Paused at 14% strain increase*

Fig. 15 shows the longitudinal strain increase versus the number of fatigue cycles for the specimens paused at 14%. The horizontal dashed line indicates the moment where the samples were paused. One of the paused specimens has a noticeably faster strain increase than the others. Also, it is observed that the impacted specimens have a slight jump in strain after impact, after which the strain increase is similar to the other samples again.

The longitudinal ε_{yy} surface strain field of specimen 45 (top) and the impacted specimen 41 (bottom) is shown in Fig. 16. The top two images show specimen 45 right before and after pause without impact, and the bottom images show specimen 41 right before and after impact. The bottom row clearly shows the impact location where the paint chipped away. However, it seems to be no effect on the strain around the hole. The transverse surface ε_{xx} strains, shown in Fig. 17, tell a similar story. Furthermore, Fig. 18a,b present the C-scan images of specimen 15 and specimen 28 which were paused at 14% strain increase and impacted at 14% strain increase respectively. It appears that the impact event does cause damage below the hole, see Fig. 17b but apparently does not noticeably influence the strain fields and the damage already present at the right and left side of the hole due to fatigue.

Figs. 19 and 20 present the cumulative AE energy and cumulative number of AE hits respectively. Although there is no clear distinction between the AE activity for the two categories of specimens, with and without impact, one could notice that accumulated energy and number of hits are higher for the impacted specimens. As it was shown with C-scan analysis, a damage area below the hole and outside the fatigue damage propagation zone is created for the impacted specimens. This area still emits AE elastic waves due to friction between the delaminated plies that is recorded by the two sensors. This phenomenon can explain the relative higher AE activity.

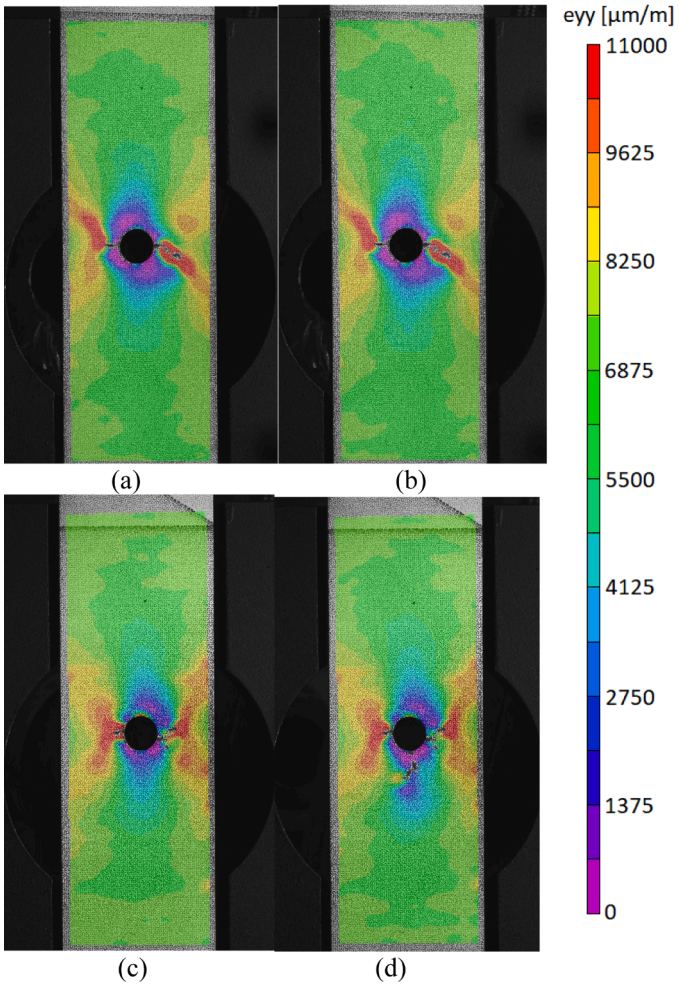

Fig. 22. Longitudinal surface e_{yy} strain for samples paused (top, specimen 23) and impacted (bottom, specimen 47) after 20% longitudinal strain increase.

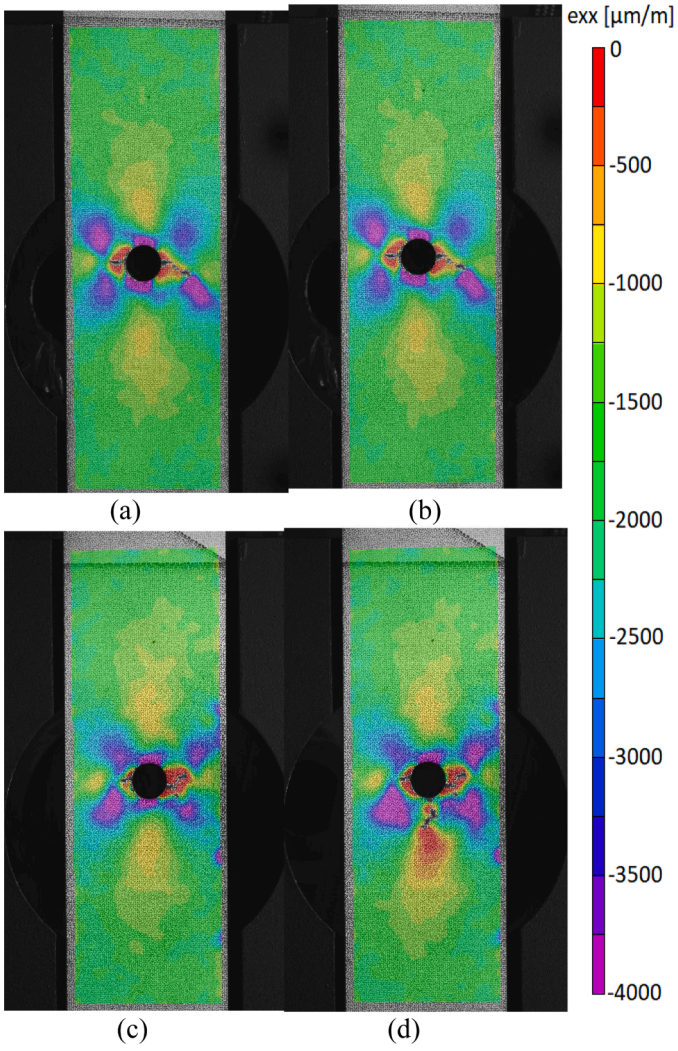

Fig. 23. Transverse surface e_{xx} strain for samples paused (top, specimen 23) and impacted (bottom, specimen 47) after 20% longitudinal strain increase.

4.4. *Paused at 20% strain increase*

Similar to the previous results of the 14% strain increase, there is no clear distinction between the fatigue life of specimens with and without impact as Fig. 21 showcases. However, directly after the pause moment, the impacted samples make a large jump upwards within a short time span. Although the fatigue life is not necessarily shortened by impact, the strain increase is typically about 10% higher.

The longitudinal surface ε_{yy} strains are shown in Fig. 22 where no difference is seen in specimen 23 that is only paused, and aside from the actual impact location, no difference is observed for impacted specimen 47 either. Looking at the transverse surface ε_{yy} strains in Fig. 23, again the top two images don't show a difference as expected. The impacted specimen however does show some difference. Directly at the lower hole edge, a small compression zone is disappeared and some damage is seen. Also, the areas showing compressive strain to the top right, bottom left and bottom right all show an increase in area after impact.

Fig. 24 shows the C-scans of specimens 37 and 32 paused at 20% strain increase and subjected to impact respectively. The areas left and right of the hole look similar, with the addition of the large delaminated area due to impact. As it was mentioned for the C-scan analysis for the specimen of the 14% strain increase, the impact introduced damage below the hole and outside the fatigue damage propagation zone and it joined the already existing damage. Considering that the impact didn't alter the fatigue life of the specimens, it can be concluded that the impact damage didn't interfere with the fatigue damage; it just enlarged the damage area around the hole.

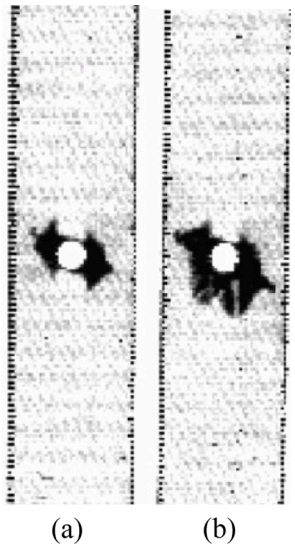

Fig. 24. C-scan images for specimens 37 paused and scanned at 20% strain increase (a) and 32 paused, impacted and scanned at 20% strain increase (b).

5. Discussion

Between the specimens that are paused and impacted at 0% strain increase (before any fatigue), a statistically significant difference in fatigue life is observed. Even with the large scatter, the life of an impacted specimen is on average a factor five shorter. The impact managed to introduce damage within the intact, at that moment, fatigue damage propagation zone and it accelerated the fatigue failure. This difference is substantiated by the various measurements performed. The strain graphs and the graphs showing cumulative AE energy release and number of AE hits show a faster damage accumulation after being hit versus being paused.

The strain field images as measured using DIC show - in addition to the damage formed at the location of impact - crack growth at the side of the hole as well. This crack then continued to grow under subsequent fatigue loading, until specimen failure. The C-scan results showed delamination formation to one side of the hole due to impact, likely on the same side as the crack formation. This delamination was triangular in shape, going outwards from the hole under $\pm 45^{\circ}$ angles. The damage evolution observed for these specimens are in a good agreement with the damage evolution reported in literature from other researchers, see for example [14,16].

In contrast, significant differences in fatigue life are not observed between the paused and impacted specimens at 14% and 20% strain increase respectively. This is reflected in the measurements as well. While the DIC strain fields and C-scans show the damage caused by impact below the hole, either no or only very small changes to the strain field, crack size or delaminated area to the sides of the hole, which is the fatigue damage propagation zone, are seen. The strain graphs show a jump in strain after impact, but the final failure strain is also higher. This makes sense as the total damaged area is unquestionably larger. Apparently, this damage does not influence the damage severity and it does not interact with the already existed damage due to fatigue in reducing the fatigue life. It could be that the fatigue damage somehow supresses some of the detrimental effects of the impact event.

Conclusions

The purpose of this paper was to investigate experimentally the effects of the timing of impact on the fatigue life and damage accumulation process for open-hole carbon fibre reinforced specimens subjected to tension-tension fatigue loading. A novel experimental set-up was designed where a mechanical testing machine was used for cyclic loading, with a gas gun positioned next to it so that specimens could be impacted in-situ. The specimens were impacted 5 mm below the central hole using aluminium tipped bullets and the impact energy used was about 10 J. Measurements were performed using a combination of digital image correlation (DIC), acoustic emission (AE) and ultrasonic C-scanning. A strain-based criterion was used to identify a common threshold for the timing of impact ensuring a fair comparison between the different tests. Three strain increase levels were identified, namely 0%, 14% and 20%, which were based on the strain increase curves measured during the fatigue tests without any impact. In total 32 fatigue tests were performed, from which 21 specimens were fatigued until failure and 11 tests were stopped at predefined time periods to be scanned. The design exercise of the experimental procedure revealed that several testing parameters should be considered, i.e. the fatigue testing parameters, the impact location, time of impact and consequently damage state of the structure, stress level within the fatigue cycle and energy of impact, geometry, shape and material of the impactor and exposed the complexity of the experimental campaign. Upon the results and discussion of the previous section, the following conclusions can be made:

- The damage areas in the paused and continuously tested samples are very similar. A difference in the pace of damage accumulation was seen however, which on average is slower when a specimen is paused. The earlier the pause in the fatigue program, the stronger this effect. During the pause, no AE hits are measured, so it is reasonable to assume no damage occurs during this time. One possibility is that the pause causes some sort of viscoelastic or creep effect in the matrix, which suppresses damage growth.
- When fatigue damage is already present, an impact event does not cause additional damage next to the hole. This differs from the pure impact case. The damage caused directly around the point of impact is however very similar. Although the damage areas overlap, they do not seem to influence each other much. The lowered stiffness around the hole due to the fatigue damage possibly reduces the transmission of impact forces through the material. The impact occurs outside of the fatigue damage propagation zone in this case.
- Although some variation is observed for individual specimens, in general it can be concluded that the fatigue damage patterns due to fatigue are similar before and after an impact. There are differences however in terms of the remaining fatigue life and how the critical damage path develops. When impacted before fatigue (at 0% strain increase), the damage level along the critical path gets a head start, and the subsequent fatigue damage increases as if serious fatigue damage was already present before. When impacted later at 14% strain increase, a slight jump in strain is seen after impact due to a decreased stiffness in the central area. Also, there is sometimes a small decrease in the number of hits and energy measured using AE after impact, but that is also observed after a pause. Finally, after a 20% strain increase, an impact causes a large jump in strain, but again the damage patterns due to fatigue are the same afterwards. This critical damage accumulates at a similar rate as after a pause at 20%.

Overall, by impacting the structure before any fatigue loading is applied, damage is introduced to the highly loaded areas next to the hole, which then grows under the subsequent cyclic loading, leading to a shortened fatigue life. The damage along the critical fatigue damage path essentially gets a head start. If the impact occurs when fatigue damage is already present, there is no significant effect on the critical damage path and fatigue life. Since the impacts were aimed outside of this fatigue damage path, the results could be very different when the impact is aimed directly at this critical zone instead as a previous study of the authors demonstrated.

This paper showcases the need to study systemically the effect of in-situ impact on the fatigue life in order to understand better the implications that may be introduced to the integrity of a composite structure. In order to achieve that further research is needed, where emphasis should be given in detecting the damage mechanisms that are present and involved and in understanding how impact could trigger their initiation or interrupt their propagation. Towards this step, X-ray technology can be used in-situ visualize in 3D the failure patterns and characterize the damage progression.

Finally, the findings of this study can be generalized, if a systematic experimental campaign is executed, taking into account all the essential testing parameters as presented in this paper.

References

[1] P. Alam, D. Mamalis, C. Robert, C. Floreani, C.M.O. Bradaigh, "The fatigue of carbon fibre reinforced plastics – a review", Compos. B. Eng. 166 (2019) 555–579.
[2] X. Li, J. Kupski, S. Texeira De Freitas, R. Benedictus, D. Zarouchas, "Unfolding the early fatigue damage process for CFRP cross-ply laminates", Int. J. Fatigue 140 (2020) 10580.
[3] A.P. Vassilopoulos, "The history of fiber-reinforced polymer composite laminate fatigue", Int. J. Fatigue 134 (2020), 105512.
[4] K.L. Reifsneider, A. Talug, "Analysis of fatigue damage in composite laminates", Int. J. Fatigue 2 (1980) 3–11.
[5] R. Sarfaraz, A.P. Vassilopoulos, T. Keller, A hybrid S-N formulation for fatigue, life modeling of composite materials and structures, Compos. Part A 43 (2012) 445–453.

[6] M. Quaresimin, L. Susmel, R. Talreja, Fatigue behaviour and life assessment of, composite laminates under multiaxial loadings, Int. J. Fatigue 32 (2010) 2–16.
[7] W. van Paepegem, J. Degrieck, A new coupled approach of residual stiffness, and strength for fatigue of fibre-reinforced composites, Int. J. Fatigue 24 (2002) 747–762.
[8] C. Kassapoglou, Fatigue of composite materials under spectrum loading, Compos. Part A 41 (2010) 663–669.
[9] M. M Shokrieh, F.T. Behrooz, A unified fatigue life model based on, energy method, Compos. Struct. 75 (2006) 444–450.
[10] S. Haojie, Y. Weixing, W. Yitao, Synergistic damage mechanic model for stiffness properties of early fatigue damage in composite laminates, Procedia Eng 74 (2014) 199–209.
[11] B. Mohammadi, H. Pakdel, Fatigue driven matrix crack propagation in laminated composites, Mater. Des. 146 (2018) 108–115.
[12] B. Mohammadi, H. Pakdel, Experimental and variational-based analytical, investigation of multiple cracked angle-ply laminates, Eng. Fract. Mech. 190 (2018) 198–212.
[13] A. Varvani-Farahani, H. Haftchenari, M. Panbechi, An energy-based fatigue damage parameter for off-axis unidirectional FRP composites, Compos. Struct. 79 (3) (2007) 381–389.
[14] EASA, "Annex II - AMC 20-29 to ED Decision 2010/003/R", tech. rep., EASA, 2010.
[15] Federal Aviation Authority. Airworthiness advisory circular, 2020, No: 20-107B Composite Aircraft Structure, [09/08/2009].
[16] J.-.M. Koo, J.-.H. Choi, C.-.S. Seok, "Evaluation for residual strength and fatigue characteristics after impact in CFRP composites", Compos. Struct. 105 (2013) 58–65.
[17] R. Bogenfeld, P. Schmiedel, N. Kuruvadi, T. Wille, J. Kreikemeier, "An experimental study of the damage growth in composite laminates under tension-fatigue after impact", Compos. Sci. Technol. 191 (2020), 108082.
[18] B. Kotter, J. Endres, J. Korbelin, F. Bittner, H.-.J. Endres, B. Fiedler. "Fatigue and fatigue after impact behaviour of thin and thick-ply composites observed by computed tomography", Composites Part C: Open Access, 100139, 2021.
[19] W. Tan, B.G. Falzon, L.N.S. Chiu, M. Price, "Predicting low velocity impact damage and compression-after-impact behaviour of composite laminates", Compos. A Appl. Sci. Manuf. 71 (2015) 212–226.
[20] E.V. Gonzalez, P. Maimi, P.P. Camanho, A. Turon, J.A. Mayugo, "Simulation of drop-weight impact and compression after impact tests on composite laminates", Compos. Struct. 94 (2012) 3364–3378.
[21] K.-.W. Kang, J.-.K. Kim, "Fatigue life prediction of impacted carbon/epoxy laminates under constant amplitude loading", Compos. A Appl. Sci. Manuf. 35 (2004) 529–535, 5.
[22] D.D. Symons, G. Davis, "Fatigue testing of impact-damaged T300/914 carbon-fibre-reinforced plastic", Compos. Sci. Technol. 60 (2000) 379–389, 2.
[23] S.R. Swanson, D.S. Cairns, M.E. Guyll, D. Johnson, "Compression fatigue response for carbon fiber with conventional and toughened epoxy matrices with damage", J. Eng. Mater. Technol. 115 (1) (1993) 116–121. Transactions of the ASME.
[24] J.-.M. Koo, J.-.H. Choi, C.-.S. Seok, "Evaluation for residual strength and fatigue characteristics after impact in CFRP composites", Compos. Struct. 105 (2013) 58–65.
[25] N.H. Tai, M.C. Yip, J.L. Lin, "Effects of low-energy impact on the fatigue behavior of carbon/epoxy composites", Compos. Sci. Technol. 58 (1) (1998) 1–8.
[26] R.C. Alderliesten, A.J. Brunner, J.A. Pascoe, "Cyclic fatigue fracture of composites: what has testing revealed about the physics of the processes so far?", Eng. Fract. Mech. 203 (2018) 186–196, 11.
[27] Vassilopoulos A.P. Fatigue life prediction of composites and composite structures, Woodhead publishing 2019.
[28] B.G. Green, M.R. Wisnom, S.R. Hallet, "An experimental investigation into the tensile strength scaling of notched composites", Compos. A Appl. Sci. Manuf. 38 (2007) 867–878.
[29] B. Aidi, M.K. Philen, S.W. Case, "Progressive damage assessment of centrally notched composite specimens in fatigue", Compos. A Appl. Sci. Manuf. 74 (2015) 47–59.
[30] G.H. Ercin, P.P. Camanho, J. Xavier, G. Catalanotti, S. Mahdi, P. Linde, "Size effects on the tensile and compressive failure of notched composite laminates", Compos. Struct. 96 (2013) 736–744.
[31] O.J. Nixon-Pearson, S.R. Hallett, P.J. Withers, J. Rouse, "Damage development in open hole composite specimens in fatigue. Part 1: experimental investigation", Compos. Struct. 106 (2013) 882–889, 12.
[32] N. Eleftheroglou, D. Zarouchas, R. Benedictus, "An adaptive probabilistic data-driven methodology for prognosis of the fatigue life of composite structures", Compos. Struct. 245 (2020).
[33] A.F. Johnson, N. Toso-Pentecote, D. Schueler, "Damage tolerance of pre-stressed composite panels under impact loads", Appl. Compos. Mater. 21 (2014) 123–147.
[34] LIBCOS Project – Significance of Load upon impact behaviour of composite structure. 2020, EASA.2009.OP.24.
[35] S.Z. Shah, S. Karuppanan, P.S. Megat-Yusoff, Z Sajid, Impact resistance and damage tolerance of fiber reinforced composites: a review, Compos. Struct. 217 (2019) 100–121, no. February, pp.
[36] M. Saeedifar, J. Mansvelder, R. Mohammadi, D. Zarouchas, "Using passive and active acoustic methods for impact damage assessment of composite structures", Compos. Struct. 226 (2019) 10.